Thermotropic Phase Behavior of Trialkyl Cyclohexanetriamides

Itsuro Tomatsu,[†] Carel F. C. Fitié,[†] Dmytro Byelov,[‡] Wim H. de Jeu,[‡] Pieter C. M. M. Magusin,[§] Michael Wübbenhorst,[||] and Rint P. Sijbesma*,[†]

Laboratory of Macromolecular and Organic Chemistry, Eindhoven University of Technology, P.O. Box 513, 5600 MB Eindhoven, The Netherlands, FOM-Institute for Atomic and Molecular Physics (AMOLF), Kruislaan 407, 1098SJ Amsterdam, The Netherlands, Schuit Institute of Catalysis, Eindhoven University of Technology, P.O. Box 513, 5600 MB Eindhoven, The Netherlands, and Laboratory of Acoustics and Thermal Physics, Department of Physics and Astronomy, Katholieke Universiteit Leuven, Celestijnenlaan 200D, B-3001 Leuven, Belgium

Received: July 29, 2009; Revised Manuscript Received: September 7, 2009

The thermotropic phase behavior of symmetric cyclohexanetriamides carrying various linear and branched alkyl chains was investigated using calorimetry, microscopy, solid-state NMR, dielectric relaxation spectroscopy, and X-ray scattering techniques. Cyclohexanetriamides carrying C_6 or longer linear alkyl chains formed columnar plastic phases with a pseudocentered rectangular lattice. Those with C_8 or longer alkyl chain also showed a nematic liquid crystalline phase. Cyclohexanetriamides carrying branched octyl chains displayed columnar phases with rectangular lattices, except for the triamide with the highly branched tetramethylbutyl group. The occurrence of less symmetrical columnar phases is ascribed to the mode of stacking of cyclohexanetriamides which leads to noncylindrical columns. Dielectric relaxation spectra also featured highly cooperative relaxation processes related to reorientation of the macrodipolar columns in the mesophase, showing the potential of these molecules as building blocks in responsive materials.

1. Introduction

The use of hydrogen bonding to form liquid crystalline (LC) materials is gathering much attention because this enhances the potential for applications such as solar cells,[1] electroconducting,[1,2] nanoporous,[3] and nanostructured materials.[4] In particular, discotic LC phases stabilized by hydrogen bonding show a higher thermal stability and responsivity for external stimuli such as electric and magnetic fields. Therefore, they are regarded as a promising systems to develop functional materials.[5,6] Among the hydrogen bonding building blocks used for self-assembly, C3 symmetrical 1,3,5-benzenetriamide (Bz-tam) is known[7−18] to form helical columnar stacks through 3-fold hydrogen bonding between molecules. This self-assembly motif is not only found in LC phases but also in solution[9,14,15,17,18] and in the crystal.[8] Various kinds of Bz-tam have been prepared, and the liquid crystalline behavior of several derivatives has been reported.[10,12,16]

Because of its structural similarity to Bz-tam, 1,3,5-cyclohexanetriamide (Ch-tam) is also regarded as a potential supramolecular building block.[19−27] Ch-tam's self-assemble through 3-fold interdisc hydrogen bonding into rigid columnar supramolecular polymers.[19,24] In contrast to Bz-tam's,[22,23] the hydrogen bonding amide groups are aligned along the column axis. Since Ch-tam's form stronger hydrogen bonding due to the optimum alignment of the amide groups, Ch-tam's carrying long alkyl chains such as octadecyl (C_{18}Ch) are highly effective gelators for many organic solvents.[21] Furthermore, the stronger hydrogen bonding of Ch-tam allows hydrogels to be made by employing amino acid derivatives which impart amphiphilicity to the molecules.[20,27] It is noteworthy that Ch-tam's carrying a short alkyl chain such as a hexyl chain (C_6Ch) are almost insoluble in various kinds of solvents, while Ch-tam's carrying branched dimethyloctyl chains show higher solubility but are less effective as a gelator than those with linear chains.[21] Ch-tam carrying highly branched, tetramethyl butyl groups (tmb-Ch) has been shown to have a particularly high solubility.[28]

Compared to Bz-tam's, only a few studies on the thermal properties of Ch-tam's have been reported. In 2002, Takasawa et al. reported thermal properties of C_{18}Ch.[25,26] According to this report, the compound shows thermal degradation at 140 °C and does not show LC texture under polarized microscopy below that temperature. Despite this caveat, we decided to study the thermotropic properties of a range of Ch-tam's, since their strong hydrogen bonding offers opportunities for thermotropic columnar phases with a macrodipole along the columnar axis which can be useful for responsive materials (e.g., electric field alignment, ferro- and piezoelectric materials). Herein, we report the thermotropic phase behavior of Ch-tam's carrying various alkyl groups using microscopy, calorimetry, X-ray scattering techniques, solid-state NMR spectroscopy, and dielectric relaxation spectroscopy.

2. Experimental Methods

2.1. Preparation of Trialkyl Cyclohexanetriamides (Ch-tam's). Tri(alkyl)cyclohexanetriamides were prepared by reaction of cyclohexane 1,3,5-tricarboxylic acid trichloride and alkyl amines according to the literature.[21] Representative preparative details are as follows: To a suspension of cyclohexane, 1,3,5-tricarboxylic acid (0.7 g, 3.0 mmol) in 10 mL of CH_2Cl_2, oxalyl chloride (1.1 mL, 14 mmol), and one drop of DMF were added. After stirring under reflux for 3 h, solvents were evaporated

* To whom correspondence should be addressed. E-mail: R.P.Sijbesma@tue.nl.
[†] Laboratory of Macromolecular and Organic Chemistry, Eindhoven University of Technology.
[‡] FOM-Institute for Atomic and Molecular Physics (AMOLF).
[§] Institute of Catalysis, Eindhoven University of Technology.
[||] Katholieke Universiteit Leuven.

10.1021/jp9072685 CCC: $40.75
Published on Web 10/08/2009

SCHEME 1: Chemical Structures of the Ch-tam's

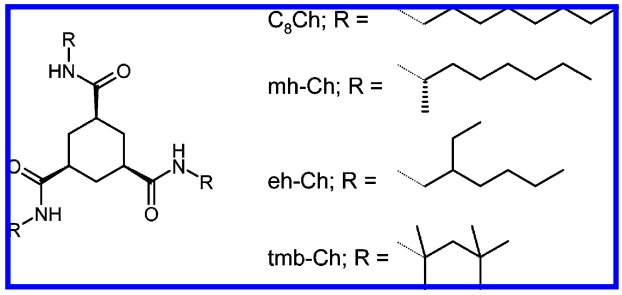

from the reaction mixture to give the tri(acid chloride). The product was used in the next reaction without further purification. Cyclohexane tricarboxylic acid trichloride (0.5 g, 1.9 mmol) was dissolved into 5 mL of $CHCl_3$ and added to a $CHCl_3$ solution of octylamine (1.0 g, 7.7 mmol) and triethyl amine (2 mL, 14 mmol). As the reaction proceeded, product precipitated from the solution. After stirring under reflux for 2 h, $CHCl_3$ was removed and the crude product was washed with water and recrystallized from $CHCl_3$/TFA. Yield: 0.79 g (74%). ^{1}H NMR (200 MHz, $CDCl_3$/TFA): $\delta = 7.10$ (b, 3H, $-NH-$), 3.30 (dt, 6H, $-NHCH_2-$), 2.63 (m, 3H, C(CO)*H*), 2.09 (m, 3H, cyclohexane), 1.78 (m, 3H, cyclohexane), 1.54 (m, 6H, $-NHCH_2CH_2-$), 1.2−1.4 (b, 30H, other CH_2), 0.88 (t, 9H, $-CH_3$). ^{13}C NMR (50 MHz, $CDCl_3$/TFA): $\delta = 177.0$, 42.2, 41.3, 31.7, 30.3, 30.0, 28.4, 28.0, 26.5, 22.5, 13.9. Calcd for $C_{33}H_{63}N_3O_3$: C, 72.03; H, 11.55; N, 7.64. Found: C, 72.13; H, 11.41; N, 7.49.

2.2. Measurements. Thermotropic phases were characterized with polarizing optical microscopy (POM), thermogravimetric analysis (TGA), differential scanning calorimetry (DSC), and wide-angle and small-angle X-ray scattering (WAXS and SAXS) techniques. TGA experiments were conducted at a rate of 10 °C/min, and POM and DSC experiments were conducted at a rate of 40 °C/min to minimize thermal degradation. All transition temperatures and enthalpies were determined from the DSC curve obtained from the first heating run. All X-ray measurements were conducted after annealing at 200 °C for 20 min. Solid-state ^{13}C-{1H} NMR (125 MHz): 8 kHz magic-angle spinning spectra at 52 °C with proton decoupling cross-polarization (CP) because of long amide relaxation time (4 mm sample holder), and static spectra between 25 and 220 °C with CP and direct excitation (7 mm sample holder; Hahn echo $2\tau = 6\ \mu$s; 5 μs 90° pulse for ^{13}C and ^{1}H). Other experimental details were described elsewhere.[4] DRS measurements were performed in a wide frequency and temperature range using a Novocontrol dielectric spectrometer. Samples were measured in the parallel plate configuration using gold plated metal electrodes (diameter 20 mm) together with quartz spacers, which ensured a stable sample geometry during the measurements in both the liquid and solid state.

3. Results and Discussion

We have chosen six linear alkyl substituents varying in length from butyl- to tetradecyl- to study the effect of chain length and three structural isomers of C_8 alkyl group, R-(-)-1-methylheptyl (mh), 2-ethylhexyl (eh), and 1,1,3,3-tetramethylbutyl (tmb), to study the effect of branching on thermotropic behavior. Ch-tam's were prepared by the conventional reaction of 1,3,5-cyclohexane tricarbonyl trichloride, with the corresponding amines,[21] and were purified by recrystallization from chloroform/TFA (see Scheme 1, C_nCh, *n* denotes the number of carbons in one alkyl chain, mh-, eh-, and tmb-Ch).

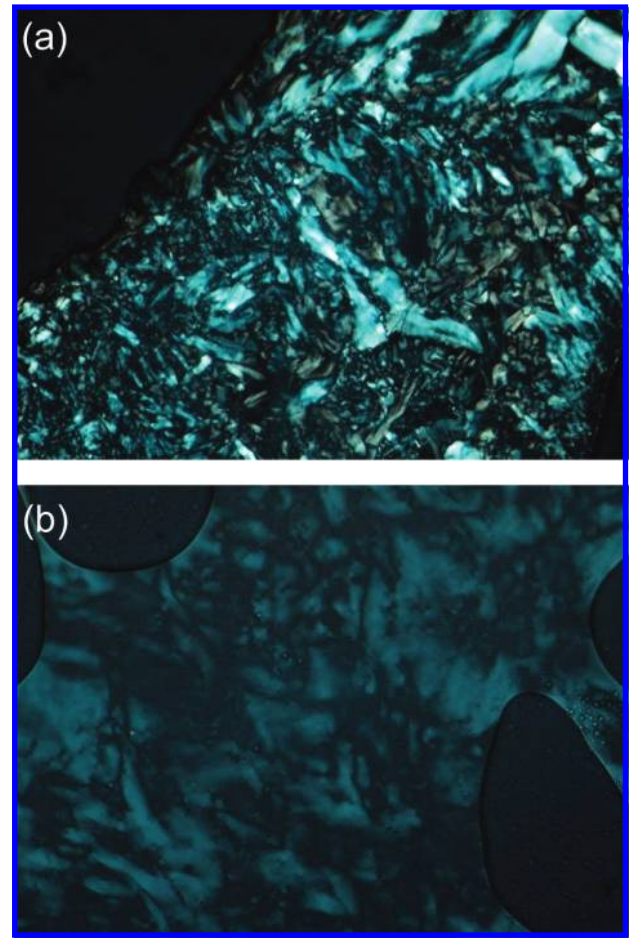

Figure 1. Micrographs of optical textures observed between crossed polarizers for C_{10}Ch at 200 °C (a) and 260 °C (b).

3.1. Ch-tam's Carrying Linear Chains. Since it is well-known that thermotropic phase behavior of LC materials strongly depends on the balance between a stiffer core and fluidic outer part, we started our investigation with Ch-tam's carrying linear chains with varying length. To evaluate the liquid crystallinity of Ch-tam's, optical textures were examined with polarizing optical microscopy (POM). In the case of C_4Ch, a transition from crystal phase to isotropic phase concurrent with thermal degradation was observed above ca. 350 °C. In the case of C_6Ch, only the isotropization was observed under POM at ca. 300 °C. However, the other molecules showed a clear change in texture between 200 and 250 °C, depending on *n*, and showed isotropization slightly above 300 °C. Typically, two distinct textures were observed, which are shown in Figure 1; at lower temperature, Ch-tam's showed bright textures, and at higher temperature, more fluid and faint textures were observed. It is noteworthy that the textures observed around 200 °C for C_{12}Ch and C_{14}Ch are barely but clearly deformable under shear.

The thermal properties of Ch-tam's were investigated with thermogravimetric analysis (TGA) and differential scanning calorimetry (DSC). Since the linear Ch-tam's did not show significant weight loss below 320 °C in TGA, DSC measurements were performed in the range from 25 to 320 °C. Endothermal peaks were seen on DSC curves consistent with transitions observed with POM. Combining the results of POM and DSC, the proposed phase sequences are summarized in Table 1. For $n = 6-14$, the isotropization temperatures are constant around 300 °C, whereas the other transitions shift to lower temperature with increasing *n*. It should be noted here

TABLE 1: Proposed Phase Sequences for C_nCh

n	transition temperatures (°C) and enthalpy changes (kJ mol^{-1})[a]
4	Cr 370[b] I
6	Cr 246 (4) Col_{rp} 297 (31) I
8	Cr 178 (13) Col_{rp} 261 (22) N 308 (4) I
10	Cr 156 (20) Col_{rp} 238 (23) N 306 (7) I
12	Cr 136 (27) Col_{rp} 226 (25) N 307 (5) I
14	Cr 129 (40) Col_{rp} 207 (5) Col 218 (15) N 305 (5) I

[a] Estimated from first heating run of DSC. [b] Estimated from POM.

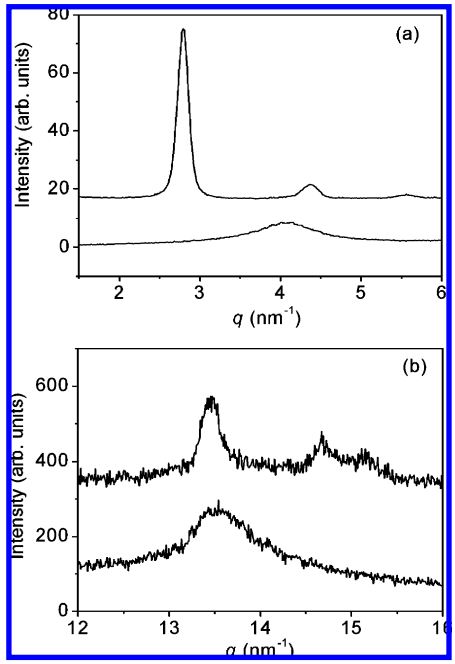

Figure 2. SAXS (a) and WAXS (b) patterns for C_8Ch for the Col_{rp} (top) and N (bottom) phases. Curves have been shifted for clarity.

that the transitions from crystalline to mesophase were observed at lower temperatures with smaller enthalpies in successive DSC runs, indicating that the crystalline samples obtained from solution had different structures than samples obtained from the melt with a cooling rate of 40 °C/min.

To investigate the structures of the phases, X-ray scattering patterns were recorded of the most important mesophases, labeled as Col_{rp} and N. As a typical example, scattering patterns for C_8Ch are shown in Figure 2. In the Col_{rp} phase, a set of several peaks was observed in both the SAXS and WAXS patterns. According to the literature,[25,26] Ch-tam's form columnar structures and resulting columns are packed into a rectangular lattice to minimize the void volume. Similar to the packing reported in the literature for Ch-tam carrying an alkylsilyl group, we propose a pseudocentered rectangular lattice for all compounds with $n = 6-14$, as shown in Figure 3.[29] This lattice allows us to explain all of the peak sets observed in the SAXS patterns for the linear alkyl substituted compounds by adjusting lattice parameters slightly. Calculated lattice parameters are listed in Table 2. Densities calculated from the lattice parameters and the molecular weight are in the expected range (0.94−0.89 g/cm^3 for $n = 6-14$), supporting the structure proposed in Figure 3. Because Ch-tam molecules in a column stack with their alkyl chains vertically above each other,[19,20,24,27] the columns have a noncircular cross section. This column shape favors a rectangular lattice with intermeshed alkyl tails as shown

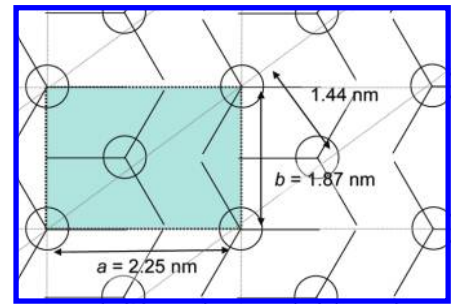

Figure 3. Proposed 2D packing structure for C_8Ch in the Col_{rp} phase.

TABLE 2: Estimated Dimensions for the Phases for C_nCh

	Col_{rp}			N[a]	
n	a (nm)	b (nm)	c (nm)	d_s (nm)	d_w (nm)
6	1.56	2.22	0.47		
8	2.25	1.87	0.47	1.54	0.46
10	2.61	1.90	0.47	1.67	0.46
12	2.98	1.91	0.47	1.79	0.46
14	3.31	1.92	0.47	1.92	0.46

[a] d_s and d_w refer to the distances calculated from the observed SAXS and WAXS maxima, respectively.

in Figure 3 instead of the hexagonal packing of cylindrical columns observed for Bz-tam's.

The WAXS patterns in the Col_{rp} phase show a strong (001) reflection related to the stacking distance between the individual Ch-tam disks in the columns and a set of weaker peaks around 15 nm^{-1} corresponding to mixed reflections such as (201) and (021) and indicating a degree of three-dimensional order of the molecules in this phase. The combination of deformability and three-dimensional order made us classify Col_{rp} as a columnar plastic phase.[30−32] This assignment is further supported by considering the correlation length along the columns in the Col_{rp} phase. From the full width at half-maximum of the (001) reflection, the correlation length was estimated to be 27 nm, significantly longer than that for Bz-tam's (ca. 5 nm) and comparable with triphenylenes in columnar plastic phases (12−30 nm).[33,34]

Additional proof for the phase assignment comes from variable temperature solid-state NMR experiments on C_{12}Ch (Figure 4, top). Comparison of spectra a and b shows that the ^{13}C NMR signals of the C_{12}Ch material in the static spectra at 52 °C are strongly broadened by chemical-shift anisotropy (CSA), which is typical of rigid materials without internal mobility. The amide signal (170 ppm) has large CSA and is therefore broadened beyond detection. At increasing temperature, the C_{12} chains become more mobile, as reflected by the reduced line width of the signals in the 10−40 ppm range. At 160 °C, the cyclohexane signals at 50 ppm are more pronounced in spectra recorded with cross-polarization (c) than with direct excitation (d). Since cross-polarization particularly enhances the ^{13}C NMR signals of protonated carbons in rigid materials, this indicates that the cyclohexane ring is immobile compared to the C12 chains (10−40 ppm). The mobility of the C_{12} chain increases further upon raising the temperature to 220 °C (e). In fact, as a result of the high C_{12} mobility at 220 °C, the NMR linewidths of the C_{12} signals approach those in the magic-angle spinning (MAS) spectrum at 52 °C. Likewise, if the triamide cyclohexane rings would be equally mobile at this temperature, an amide signal similar to that in the MAS spectrum would be expected in the static spectrum at 220 °C, which is not the case.

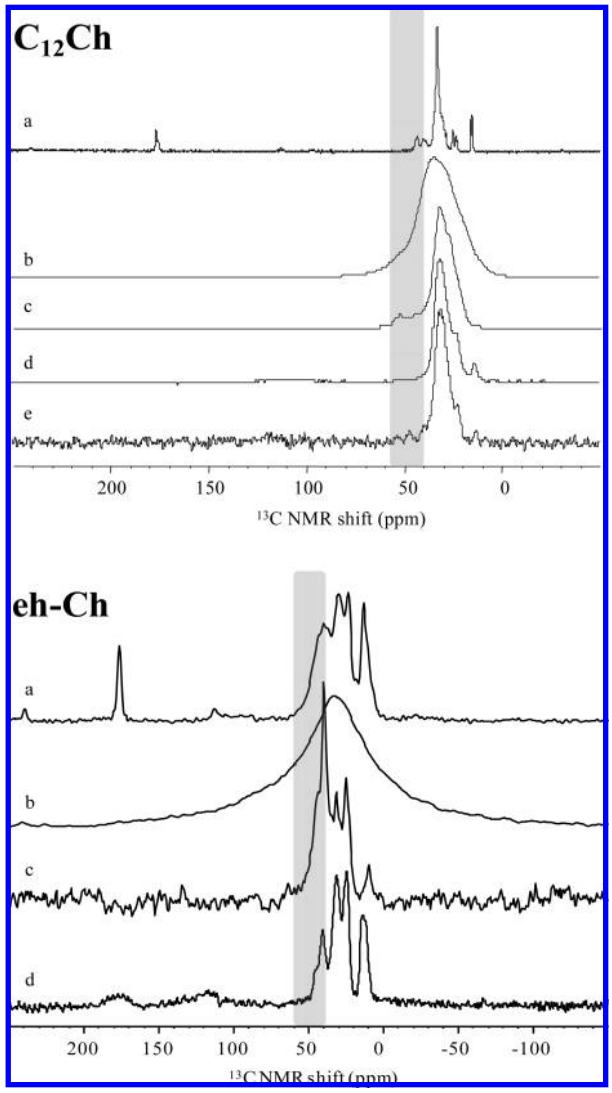

Figure 4. Solid-state ^{13}C NMR spectra for $C_{12}Ch$ (top) and eh-Ch (bottom). The gray rectangles indicate the regions featuring signals from the cyclohexane core. (top) Proton-decoupled ^{13}C NMR spectra of $C_{12}Ch$ at varied temperature (a) with and (b−e) without sample rotation. (a, b) Cross-polarization spectra at 52 °C, (c) cross-polarization and (d) direct-excitation spectra at 160 °C, and (e) direct-excitation spectrum at 220 °C. (bottom) Proton-decoupled ^{13}C NMR spectra of eh-Ch at varied temperature (a) with and (b−d) without sample rotation. (a, b) Cross-polarization spectra at 52 °C and (c) cross-polarization and (d) direct-excitation spectra at 160 °C. The signal at 125 ppm in the eh-Ch spectrum (e) originates from the Teflon spacer inside the NMR sample holder.

The NMR invisibility of the cyclohexane signals and amide signal at 220 °C indicates that the triamide cyclohexane ring is still immobile at this temperature, as is consistent with the picture of the Col_{rp} phase consisting of rigid cores and fluidic outer parts.

In the N phase, single broad peaks were observed in both the SAXS and WAXS patterns, as shown in Figure 2. From the SAXS and WAXS maxima, the corresponding distances d_s and d_w were calculated for $n = 8-14$ and listed in Table 2. Since the Ch-tam's in this phase were fluidic and the broad peak shapes are characteristic for a disordered phase, we can classify the N phase as a nematic phase. This is also supported by the calculated spacings which are consistent with the dimensions of the molecules estimated by assuming a disk-like shape.

TABLE 3: Proposed Phase Sequences for Ch-tam's with Branched Chains

R	transition temperatures (°C) and enthalpy changes (kJ mol^{-1})[a]
mh-	Cr_1 240 (3) Cr_2 271 (7) Col 340[b] I
eh-	Cr 142 (18) Col_{rp} 187 (2) Col_1 222 (-) Col_2 330[b] I
tmb-	Cr_1 229 (5) Cr_2 287 (1) Cr_3 340[b] I

[a] determined by first heating run of DSC. [b] determined by POM.

3.2. Ch-tam's Carrying Branched C_8 Chains. Since the observations for C_nCh indicate that positional correlation between alkyl chains belonging to neighboring molecules plays an important role in the phase behavior, it is expected that structural modification in the alkyl chains will result in a different packing efficiency and, thus, in a different mesophase structure. Therefore, three Ch-tam's carrying branched alkyl groups consisting of eight carbons were prepared (Scheme 1: mh-Ch, eh-Ch, and tmb-Ch).

The phase behavior of these Ch-tam's was also evaluated from their optical textures under POM. In the case of tmb-Ch, the crystal phase showed a direct transition to the isotropic phase with thermal degradation around 340 °C.[28] Both mh-Ch and eh-Ch did show mesophases, as evidenced by the appearance of textures starting at 275 and 150 °C, respectively, and a transition to the isotropic phase with degradation at 330−340 °C. In contrast to the nonbranched C_8Ch, which shows two mesophases with different textures under POM, only a single, shear, deformable texture was observed for both mh- and eh-Ch. DSC measurements were also performed in the range from 30 to 320 °C, and endothermal peaks were observed at 271 °C for mh-Ch and 142 °C for eh-Ch, in agreement with the transitions observed with POM. In addition, a number of smaller endothermal peaks were observed at 240 °C for mh-Ch and 187 and 222 °C for eh-Ch, which did not correspond with transitions visible in POM. Combining the results of POM and DSC, the proposed phase sequences are summarized in Table 3.

To elucidate the mesophase structures, X-ray scattering patterns were recorded for mh- and eh-Ch. As shown in Figure 5, both compounds display a single peak in the WAXS pattern and do not show a peak in the smaller q-range (<3 nm^{-1}) in the SAXS pattern, which can be seen in the case of linear C_8Ch. Since the scattering patterns for branched mh- and eh-Ch are similar to those reported in the literature,[25,26] intercolumn distances are estimated (Table 4) assuming a pseudorectangular lattice, as shown in Figure 6. The packing structures of the columns for branched Ch-tam's have higher symmetry than that for nonbranched C_8Ch because branched chains are distributed more equally around the cyclohexane core.

Concerning the nature of the mesophases observed for mh-Ch and eh-Ch, the situation is rather different from the case of the linear Ch-tam's. Although both branched compounds show barely shear deformable textures under POM, the WAXS patterns do not show mixed reflections that can be attributed to the enhanced three-dimensional order commonly observed in plastic columnar phases. Since eh-Ch is best soluble and thus processable and displays the richest phase behavior of all ch-tam's included in this study, we decided to investigate the nature of the mesophases formed by this compound in more detail by solid-state NMR and dielectric relaxation spectroscopy (DRS).

3.3. Solid-State NMR and DRS Characterization of eh-Ch. Similar solid-state NMR measurements were conducted for eh-Ch as for the linear $C_{12}Ch$ in the crystalline (Cr, 52 °C) and the lowest temperature mesophase (Col_{rp}, 160 °C), but not in the Col_1 and Col_2 phase, due to temperature limitations of the

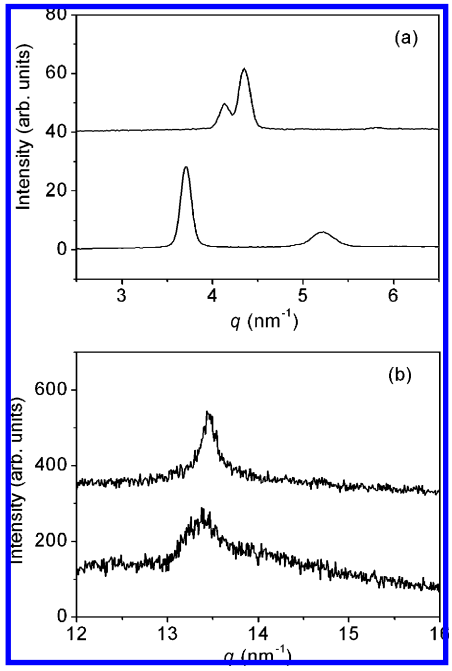

Figure 5. SAXS (a) and WAXS (b) patterns for mh-Ch at 290 °C (upper) and eh-Ch at 170 °C (lower). Curves have been shifted for clarity.

TABLE 4: Estimated Dimensions for the Mesophases for mh- and eh-Ch

	T (°C)	phase	intercolumn distance (nm)		disk−disk distance (nm)
mh-Ch	290	Col	1.53	1.46	0.47
eh-Ch	170	Col_{rp}	1.70	1.23	0.47
eh-Ch	270	Col_2	1.45	1.45	0.46

NMR setup (Figure 4, bottom). The ^{13}C NMR signals in the static spectra in the crystalline state at 52 °C are more strongly broadened by CSA than in the case of $C_{12}Ch$, while the MAS spectrum at the same temperature has a narrow line width even for the amide carbon around 170 ppm. In the low temperature mesophase Col_{rp} at 160 °C, the line width of all signals between 0 and 50 ppm is strongly reduced irrespective of the excitation method used, reflecting the higher overall mobility of this phase. The signals corresponding to the cyclohexane core (40−50 ppm) are much more pronounced in the cross-polarization spectrum (c) than in the direct-excitation spectrum (d), and the amide carbon signal is broadened beyond detection in both spectra. These observations clearly show that the cyclohexane ring is much less mobile compared to the branched alkyl chains in the

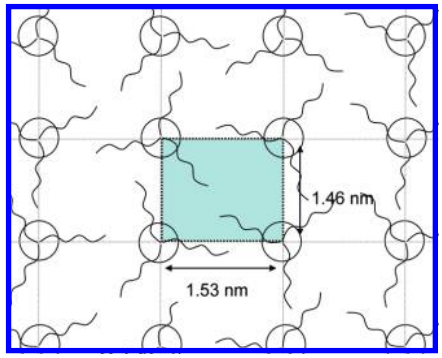

Figure 6. Proposed 2D packing structure for mh-Ch in the Col_{rp} phase.

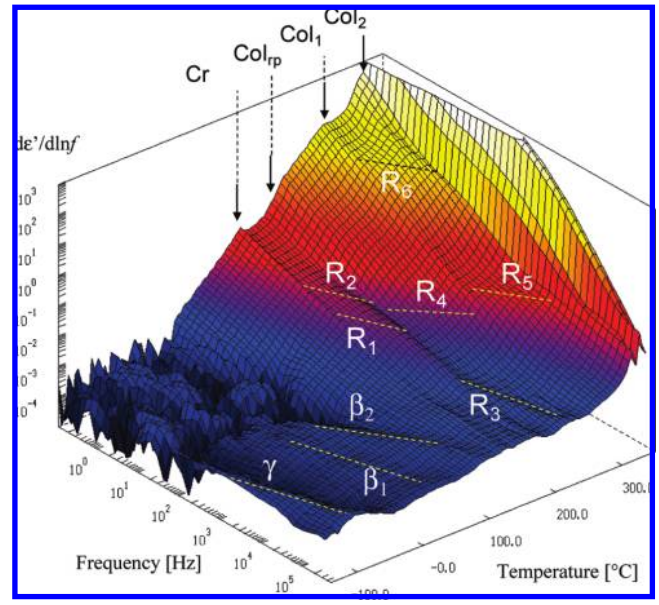

Figure 7. Dielectric spectrum for eh-Ch. The dielectric spectrum is plotted as $d\varepsilon'/d \ln f$ according to ref 36. All dielectric relaxation processes are marked by dotted lines and labeled as in Table 5. The phase transitions are indicated by arrows, and the phases are labeled on top.

low temperature mesophase of eh-Ch. However, where the cyclohexane signals are undetectable in the direct-excitation spectrum at 160 °C for $C_{12}Ch$, these signals are clearly discernible for eh-Ch (spectrum d, top and bottom). Even the amide signal at 170 ppm starts to show up in the static direct-excitation spectrum of eh-Ch at 160 °C. These differences indicate that the cyclohexane rings are relatively more mobile in the low temperature mesophase of eh-Ch than in $C_{12}Ch$. These observations are also consistent with the WAXS pattern recorded for eh-Ch in which mixed reflections related to enhanced three-dimensional order between the cyclohexane cores are absent. On the basis of POM, WAXS, and these NMR results, we classify the lowest temperature mesophase of eh-Ch as a plastic crystal and the two higher temperature phases as two different columnar mesophases.

In general, DRS probes the interaction of electromagnetic waves with matter in the frequency regime between 10^{-6} and 10^{12} Hz. Dielectric relaxations, that is, dielectric dispersion and absorption in solid insulating materials and polar liquids, occurring in this frequency range can be linked to reorientational motions of molecular dipoles and charge transport in such materials.[35] Large macrodipoles occur in self-assembled Ch-tam gels due to the alignment of the three hydrogen bonded amides along the columnar axis.[22] Therefore, investigation of the dipolar relaxations in eh-Ch by means of DRS is ideally suited to gain more insight in both the dynamic nature of the high temperature mesophases and the molecular processes in which the amide bonds are involved. DRS measurements were performed between −140 and 350 °C upon cooling from the isotropic melt in a frequency range from 10^{-1} to 10^{6} Hz (Figure 7). A total of nine relaxation processes were observed in the dielectric spectra, and their characteristic relaxation times and thermal activation parameters (Arrhenius behavior) were determined using a fitting procedure described elsewhere.[36] Additionally, from the Arrhenius parameters, the activation enthalpy and entropy for all processes were computed using the Starkweather analysis.[37]

3.3.1. Phase Behavior. When looking at the activation plot of all relaxation processes and the measured conductivity as a

TABLE 5: Activation Parameters for All Relaxation Processes in eh-Ch

process	phase	$\log(\tau_0)$ (s)	E_a (kJ mol^{-1})	ΔH^a (kJ mol^{-1})	ΔS^a (J mol^{-1} K^{-1})
γ	Cr	−13.7	25	23	18
β_1	Cr	−13.4	45	43	7
β_2	Cr	−14.5	62	56	27
R_1	Col_{rp}	−19.6	143	96	119
R_2	Col_{rp}	−17.9	138	102	87
R_3	Col_1	−26.6	195	95	254
R_4	Col_1	−12.4	86	93	−18
R_5	Col_2	−13.7	107	104	7
R_6	Col_2	−11.8	108	124	−31

[a] Calculated based on the Starkweather analysis.

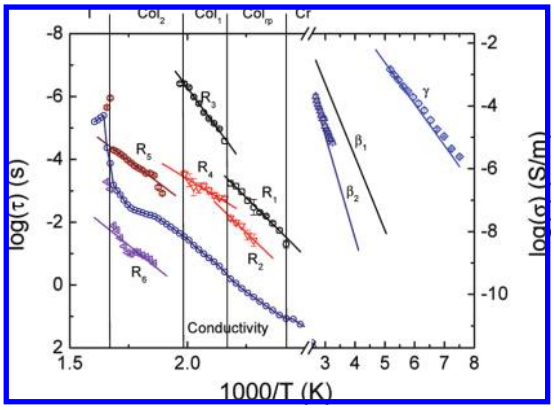

Figure 8. Activation plot for all dielectric relaxation processes in eh-Ch (relaxation time τ, left axis) and conductivity (σ, right axis) as a function of inverse temperature.[38] The relaxation processes are labeled as in Table 5, and the phase regions are indicated by vertical lines and labeled on top.

function of temperature, four clear discontinuities are apparent that correspond very well to the phase transition temperatures measured by DSC and POM (Figure 8).

3.3.2. Relaxation Processes in the Cr Phase. In the crystalline phase, three fast relaxation processes are present with an Arrhenius-type thermal activation (γ, β_1, and β_2).[37] All three processes occur well below room temperature and are characterized by low activation energy barriers favoring an assignment to local molecular motions in the system. The activation energy (E_a) of about 25 kJ mol^{-1} for the lowest temperature process matches very well E_a values found for γ-relaxations reported for other systems with a high amide content such as oligopeptides, various nylons, and hyperbranched polyamides based on discotic moieties.[39−43] As for these systems, the γ-relaxation for eh-Ch can be attributed to local motion of the alkyl chains connected to the amide bonds. In further accordance with the literature, both β-relaxations appear at higher temperature and have an activation energy that is roughly twice as high as that of the γ-relaxation. The β-relaxation is generally attributed to local rotations of hydrogen bonded or non-hydrogen-bonded amide groups. Since all known crystal structures for Ch-tam's with alkyl substituents feature intramolecular hydrogen bonds for all three amides, we tentatively assign the two β-relaxations to local rotations of the hydrogen bonded amides and non-hydrogen-bonded amide species resulting from defects in the crystalline structure.[44]

3.3.3. Relaxation Processes in the Col_{rp} Phase. In the lowest temperature mesophase, two slower processes are observed with very high activation energies (R_1 and R_2). Moreover, the calculated activation entropy for both processes is very high, indicating that these processes are associated with strongly cooperative molecular motions. The presence of these collective motions involving longer length scales clearly demonstrates the enhanced mobility of the Col_{rp} phase over the crystalline state and is consistent with POM and solid-state NMR results. Slow and cooperative processes have been reported earlier for columnar mesophases at higher temperatures, which were assigned to collective reorientations of whole (short) columns and, alternatively, to macrodipole inversions by collective 180° reorientational jumps of polar groups within the columnar structure.[45,46] Given the hydrogen bonded columnar structure of eh-CH in its mesophases, both of the proposed relaxation modes can be envisioned, although a conclusive assignment is not possible solely based on the dielectric relaxation data.

3.3.4. Relaxation Processes in the Col_1 and Col_2 Phase. In the Col_1 phase, there are two highly activated processes present (R_3−R_4). While the activation entropy for R_4 is very low, the activation entropy for the R_3-relaxation is even substantially higher than those for the collective relaxations in the Col_{rp} phase. The activation parameters imply that one of the proposed collective relaxation modes that is operative in the Col_{rp} phase becomes not only faster but, intriguingly, also more cooperative in the higher temperature mesophase Col_1. Speeding up the relaxation processes can be explained by the increase in mobility and disorder in the higher temperature mesophase, but to explain the observed increase in cooperativity, a more detailed investigation of the relaxation mechanism would be required, which is beyond the scope of this study.

In the Col_2 phase, mobility has increased to such an extent that no collective relaxation processes are present anymore. The two processes (R_5−R_6) that have been identified in this phase are both highly activated but have a very low or negative activation entropy. The exact molecular basis for the R_5-relaxation remains unclear, but process R_6 is most probably a charge relaxation due to its strong correlation with the temperature dependence of the electrical conductivity (Figure 8).

3.4. Comparison with Bz-tam's. The ordering of Ch-tam's in thermotropic phases is significantly different from Bz-tam's,[10] although their chemical structures are related. In the case of Bz-tam's carrying linear C_5−C_{18} alkyl chains, the transitions from the crystalline phase to the mesophase are observed between 49 and 119 °C and the transition to the isotropic liquid occurs already around 210 °C. In contrast to the plastic mesophases observed for Ch-tam, X-ray scattering measurements show that these Bz-tam's form disordered hexagonal columnar liquid crystalline phases, in which columns are formed by helical stacking of molecules.[8,10] As seen in comparison of solution properties between Ch-tam and Bz-tam,[19,24] the appearance of more ordered mesophases and higher isotropization temperatures for Ch-tam's are due to the strong tendency to form straight columns with ideal orientation of amide groups for hydrogen bonding interaction. This tendency provides a stiffer, nonhelical columnar structure to Ch-tam's in which the alkyl chains are not distributed evenly around the core. This, in turn, prevents the formation of hexagonal columnar phases even for the derivatives carrying branched chains.

4. Conclusion

The thermotropic phase behavior of a range of Ch-tam's carrying various alkyl groups has been established. Ch-tam's carrying linear chains with $n \geq 6$ show columnar plastic phases in which molecules self-assemble in a columnar structure and the resulting columns are packed in a pseudocentered rectangular lattice, while CH-tam's with longer linear alkyl chains ($n \geq 8$) show nematic LC phases. If the Ch-tam carries C_8 branched

chains, columnar mesophases with a pseudorectangular lattice are observed except for the one carrying highly branched tmb groups, which did not show any mesophase. The less symmetrical structures are due to the straight stacking of Ch-tam's through hydrogen bonding, leading to high orientational correlation between alkyl chains and a noncylindrical column shape. Dielectric relaxation spectroscopy for the branched eh-Ch derivative also provided clear evidence for highly cooperative relaxation processes related to reorientation of the macrodipolar Ch-tam columns in the mesophase. These results underline the potential of Ch-tam's to be used as a highly stable building block in the design of responsive materials (e.g., electric field alignment, ferro- and piezoelectric materials).

Acknowledgment. The authors thank Dr. Xianwen Lou for MALDI-TOF-MASS, Mr. Henk Eding for elemental analysis, Mr. Brahim Mezari for his assistance with the NMR experiments, and Ms. Esther Vinken for TGA measurement. The X-ray work at the FOM Institute for Atomic and Molecular Physics is part of the research program of the "Stichting voor Fundamenteel Onderzoek der Materie (FOM)", which is financially supported by the "Nederlandse Organisatie voor Wetenschappelijk Onderzoek (NWO)".

Supporting Information Available: X-ray scattering, TGA, and DSC data. This material is available free of charge via the Internet at http://pubs.acs.org.

References and Notes

(1) Laschat, S.; Baro, A.; Steinke, N.; Giesselmann, F.; Hagele, C.; Scalia, G.; Judele, R.; Kapatsina, E.; Sauer, S.; Schreivogel, A.; Tosoni, M. *Angew. Chem., Int. Ed.* **2007**, *46*, 4832–4887.

(2) Palmans, A. R. A.; Vekemans, J. A. J. M.; Hikmet, R. A.; Fischer, H.; Meijer, E. W. *Adv. Mater.* **1998**, *10*, 873.

(3) Zhou, M. J.; Kidd, T. J.; Noble, R. D.; Gin, D. L. *Adv. Mater.* **2005**, *17*, 1850.

(4) Fitié, C. F. C.; Tomatsu, I.; Byelov, D.; de Jeu, W. H.; Sijbesma, R. P. *Chem. Mater.* **2008**, *20*, 2394–2404.

(5) Bushey, M. L.; Nguyen, T. Q.; Nuckolls, C. *J. Am. Chem. Soc.* **2003**, *125*, 8264–8269.

(6) Nguyen, T. Q.; Martel, R.; Bushey, M.; Avouris, P.; Carlsen, A.; Nuckolls, C.; Brus, L. *Phys. Chem. Chem. Phys.* **2007**, *9*, 1515–1532.

(7) Bose, P. P.; Drew, M. G. B.; Das, A. K.; Banerjee, A. *Chem. Commun.* **2006**, 3196–3198.

(8) Lightfoot, M. P.; Mair, F. S.; Pritchard, R. G.; Warren, J. E. *Chem. Commun.* **1999**, 1945–1946.

(9) Masuda, M.; Jonkheijm, P.; Sijbesma, R. P.; Meijer, E. W. *J. Am. Chem. Soc.* **2003**, *125*, 15935–15940.

(10) Matsunaga, Y.; Miyajima, N.; Nakayasu, Y.; Sakai, S.; Yonenaga, M. *Bull. Chem. Soc. Jpn.* **1988**, *61*, 207–210.

(11) Ogata, D.; Shikata, T.; Hanabusa, K. *J. Phys. Chem. B* **2004**, *108*, 15503–15510.

(12) Paraschiv, I.; Giesbers, M.; van Lagen, B.; Grozema, F. C.; Abellon, R. D.; Siebbeles, L. D. A.; Marcelis, A. T. M.; Zuilhof, H.; Sudholter, E. J. R. *Chem. Mater.* **2006**, *18*, 968–974.

(13) Shikata, T.; Ogata, D.; Hanabusa, K. *J. Phys. Chem. B* **2004**, *108*, 508–514.

(14) van der Schoot, P.; Michels, M. A. J.; Brunsveld, L.; Sijbesma, R. P.; Ramzi, A. *Langmuir* **2000**, *16*, 10076–10083.

(15) van Gestel, J.; Palmans, A. R. A.; Titulaer, B.; Vekemans, J. A. J. M.; Meijer, E. W. *J. Am. Chem. Soc.* **2005**, *127*, 5490–5494.

(16) van Gorp, J. J.; Vekemans, J. A. J. M.; Meijer, E. W. *J. Am. Chem. Soc.* **2002**, *124*, 14759–14769.

(17) Wilson, A. J.; Masuda, M.; Sijbesma, R. P.; Meijer, E. W. *Angew. Chem., Int. Ed.* **2005**, *44*, 2275–2279.

(18) Wilson, A. J.; van Gestel, J.; Sijbesma, R. P.; Meijer, E. W. *Chem. Commun.* **2006**, 4404–4406.

(19) Fan, E. K.; Yang, J.; Geib, S. J.; Stoner, T. C.; Hopkins, M. D.; Hamilton, A. D. *J. Chem. Soc., Chem. Commun.* **1995**, 1251–1252.

(20) Friggeri, A.; van der pol, C.; van Bommel, K. J. C.; Heeres, A.; Stuart, M. C. A.; Feringa, B. L.; van Esch, J. *Chem.—Eur. J.* **2005**, *11*, 5353–5361.

(21) Hanabusa, K.; Kawakami, A.; Kimura, M.; Shirai, H. *Chem. Lett.* **1997**, 191–192.

(22) Sakamoto, A.; Ogata, D.; Shikata, T.; Hanabusa, K. *Macromolecules* **2005**, *38*, 8983–8986.

(23) Sakamoto, A.; Ogata, D.; Shikata, T.; Urakawa, O.; Hanabusa, K. *Polymer* **2006**, *47*, 956–960.

(24) Shikata, T.; Ogata, D.; Hanabusa, K. *Nihon Reoroji Gakkaishi* **2003**, *31*, 229–236.

(25) Takasawa, R.; Murota, K.; Yoshikawa, I.; Araki, K. *Macromol. Rapid Commun.* **2003**, *24*, 335–339.

(26) Takasawa, R.; Yoshikawa, I.; Araki, K. *Kobunshi Ronbunshu* **2002**, *59*, 616–622.

(27) van Bommel, K. J. C.; van der Pol, C.; Muizebelt, I.; Friggeri, A.; Heeres, A.; Meetsma, A.; Feringa, B. L.; van Esch, J. *Angew. Chem., Int. Ed.* **2004**, *43*, 1663–1667.

(28) Raposo, C.; Perez, N.; Almaraz, M.; Mussons, M. L.; Caballero, M. C.; Moran, J. R. *Tetrahedron Lett.* **1995**, *36*, 3255–3258.

(29) Although we were not sure of the packing of the alkyl chains, we drew a possible arrangement of the alkyl chains in order to clarify our proposed structure.

(30) Glusen, B.; Heitz, W.; Kettner, A.; Wendorff, J. H. *Liq. Cryst.* **1996**, *20*, 627–633.

(31) Li, J.; Kastler, M.; Pisula, W.; Robertson, J. W. F.; Wasserfallen, D.; Grimsdale, A. C.; Wu, J.; Mullen, K. *Adv. Funct. Mater.* **2007**, *17*, 2528–2533.

(32) Simmerer, J.; Glusen, B.; Paulus, W.; Kettner, A.; Schuhmacher, P.; Adam, D.; Etzbach, K. H.; Siemensmeyer, K.; Wendorff, J. H.; Ringsdorf, H.; Haarer, D. *Adv. Mater.* **1996**, *8*, 815–819.

(33) Brandl, B.; Wendorff, J. H. *Liq. Cryst.* **2005**, *32*, 425–430.

(34) Prasad, S. K.; Rao, D. S. S.; Chandrasekhar, S.; Kumar, S. *Mol. Cryst. Liq. Cryst.* **2003**, *396*, 121–139.

(35) Kremer, F.; Schönhals, A. *Broadband dielectric spectroscopy*; Springer: Berlin, Germany, 2003.

(36) Wübbenhorst, M.; van Turnhout, J. *J. Non-Cryst. Solids* **2002**, *305*, 40–49.

(37) Starkweather, H. W. *Macromolecules* **1981**, *14*, 1277–1281.

(38) For a more detailed analysis of the γ/β region, a two-dimensional fit procedure based on the whole $\varepsilon''(f, T)$ data set to three HNArrh functions was applied (see ref 36), which revealed a third process (β_1) along with a good reproduction of the conventionally fitted β_2- and γ-relaxations. Since this procedure yields the Arrhenius parameters directly, the results are displayed as the three rightmost straight lines in Figure 8.

(39) Avakian, P.; Matheson, R. R.; Starkweather, H. W. *Macromolecules* **1991**, *24*, 4698–4700.

(40) Emran, S. K.; Newkome, G. R.; Weis, C. D.; Harmon, J. P. *J. Polym. Sci., Part B: Polym. Phys.* **1999**, *37*, 2025–2038.

(41) Hakme, C.; Stevenson, I.; Fulchiron, R.; Seytre, G.; Clement, F.; Odoni, L.; Rochat, S.; Varlet, J. *J. Appl. Polym. Sci.* **2005**, *97*, 1522–1537.

(42) Huwe, K.; Appelhans, D.; Prigann, J.; Voit, B. I.; Kremer, F. *Macromolecules* **2000**, *33*, 3762–3766.

(43) Papadopoulos, P.; Floudas, G.; Klok, H. A.; Schnell, I.; Pakula, T. *Biomacromolecules* **2004**, *5*, 81–91.

(44) Stadler, R. Ludwig S. Schollmeyer D. (2004) Private communication to the Cambridge Structural Database, deposition numbers CCDC 151387, CCDC 151388, CCDC 151389.

(45) Elmahdy, M. M.; Floudas, G.; Mondeshki, M.; Spiess, H. W.; Dou, X.; Mullen, K. *Phys. Rev. Lett.* **2008**, *100*, 107801.

(46) Kilian, D.; Knawby, D.; Athanassopoulou, M. A.; Trzaska, S. T.; Swager, T. M.; Wrobel, S.; Haase, W. *Liq. Cryst.* **2000**, *27*, 509–521.

JP9072685